Supplementary material: Figures for Appendix D of the paper "Investigating 39 Galactic Wolf-Rayet stars with VLTI/GRAVITY: Uncovering a long period binary desert"

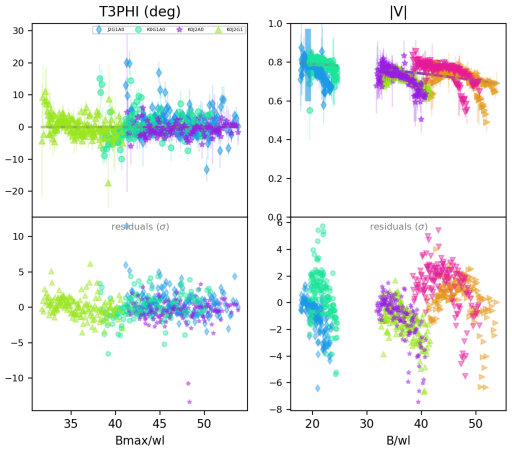

Fig. 1. |V|-T3PHI data (top panels) for WR 8 fit with a central point source + fully resolved component, along with corresponding residuals (bottom panels).

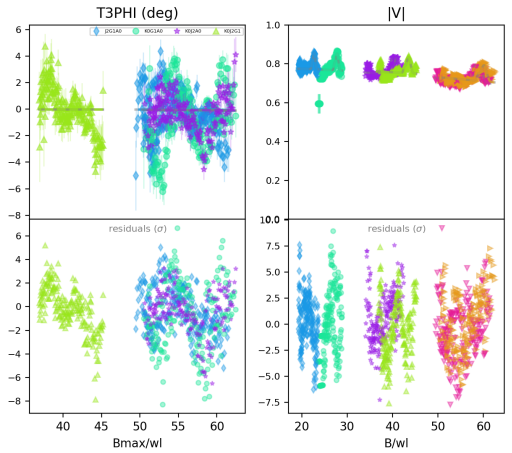

Fig. 2. |V|-T3PHI data (top panels) for WR 9 fit with a central point source + fully resolved component, along with corresponding residuals (bottom panels).

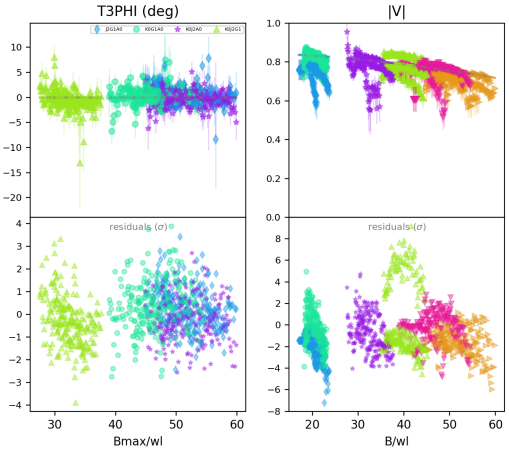

Fig. 3. |V|-T3PHI data (top panels) for WR 12 fit with a central point source + fully resolved component, along with corresponding residuals (bottom panels).

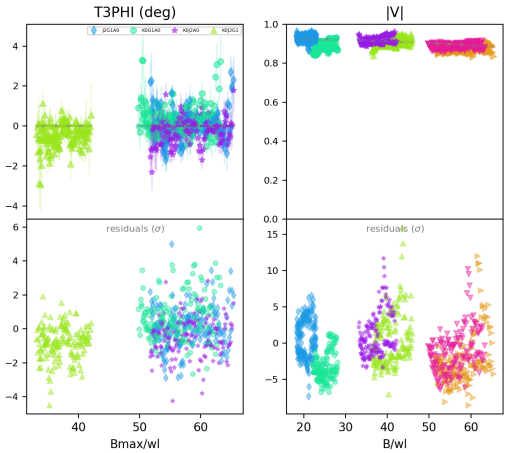

Fig. 4. |V|-T3PHI data (top panels) for WR 14 fit with a central point source + fully resolved component, along with corresponding residuals (bottom panels).

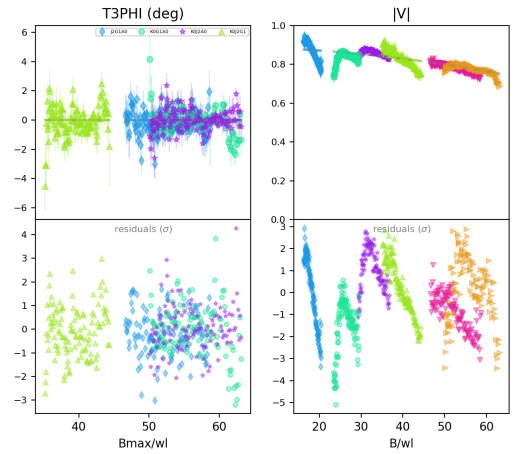

Fig. 5. |V|-T3PHI data (top panels) for WR 15 fit with a central point source + fully resolved component, along with corresponding residuals (bottom panels).

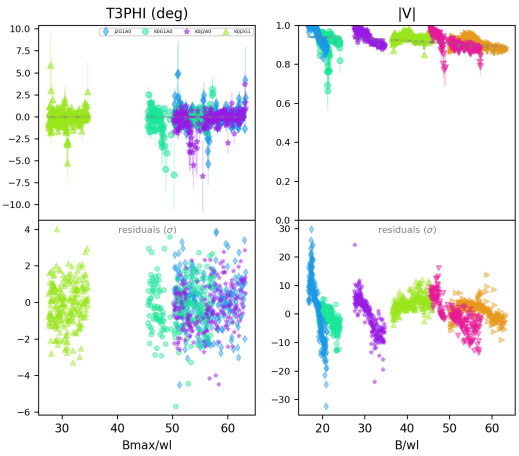

Fig. 6. |V|-T3PHI data (top panels) for WR 16 fit with a central point source + fully resolved component, along with corresponding residuals (bottom panels).

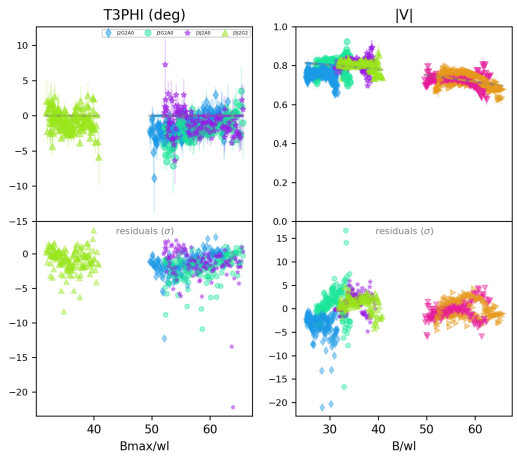

Fig. 7. |V|-T3PHI data (top panels) for WR 21 fit with a central point source + fully resolved component, along with corresponding residuals (bottom panels).

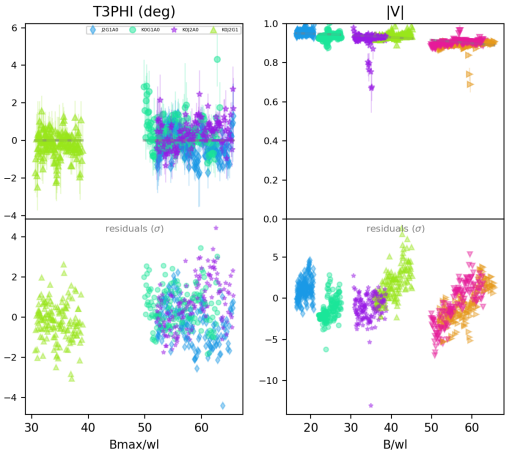

Fig. 8. |V|-T3PHI data (top panels) for WR 23 fit with a central point source + fully resolved component, along with corresponding residuals (bottom panels).

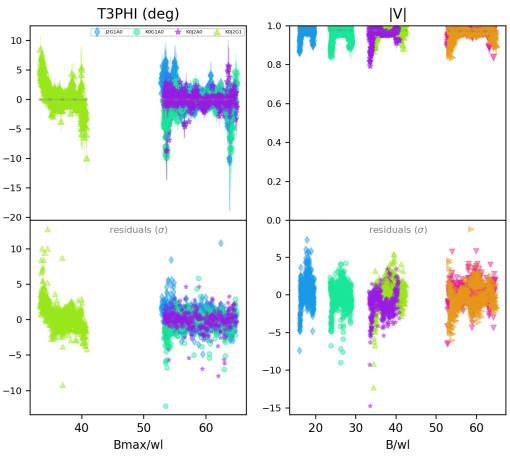

Fig. 9. |V|-T3PHI data (top panels) for WR 24 fit with a central point source + fully resolved component, along with corresponding residuals (bottom panels).

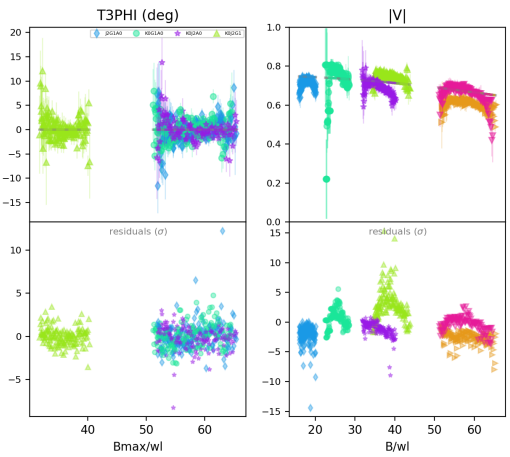

Fig. 10. |V|-T3PHI data (top panels) for WR 31 fit with a central point source + fully resolved component, along with corresponding residuals (bottom panels).

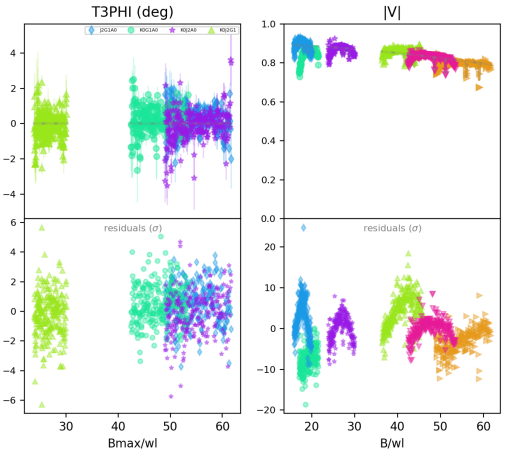

Fig. 11. |V|-T3PHI data (top panels) for WR 31a fit with a central point source + fully resolved component, along with corresponding residuals (bottom panels).

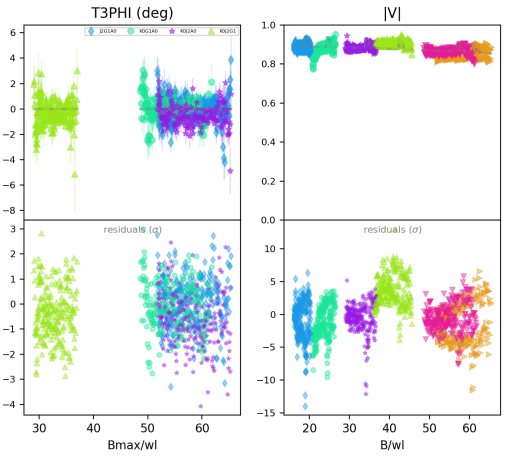

Fig. 12. |V|-T3PHI data (top panels) for WR 42 fit with a central point source + fully resolved component, along with corresponding residuals (bottom panels).

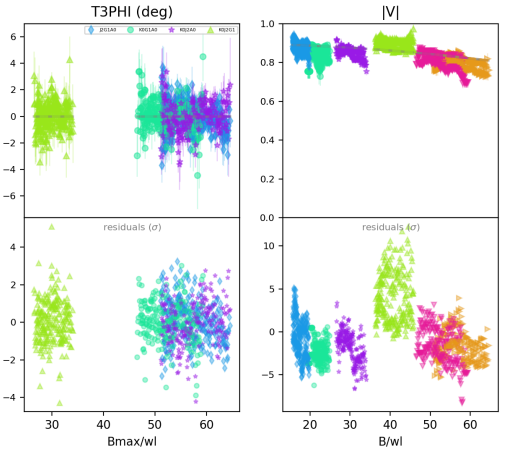

Fig. 13. |V|-T3PHI data (top panels) for WR 47 fit with a central point source + fully resolved component, along with corresponding residuals (bottom panels).

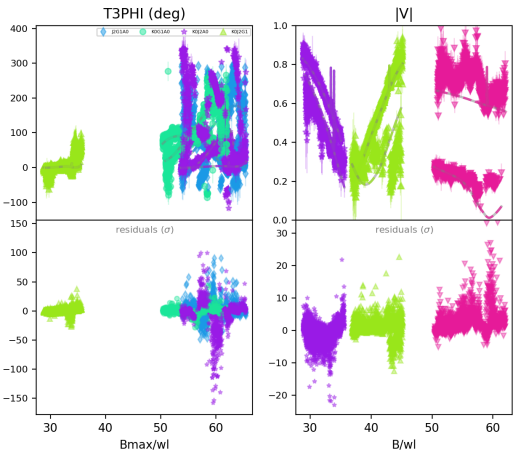

Fig. 14. |V|-T3PHI data (top panels) for WR 48 fit with two point sources to model the binary, along with a fully resolved component, and the corresponding residuals (bottom panels).

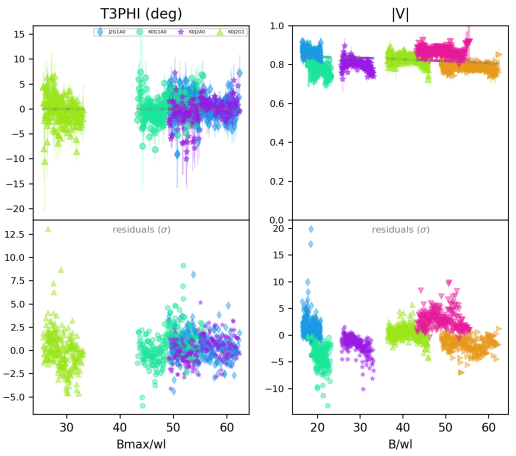

Fig. 15. |V|-T3PHI data (top panels) for WR 52 fit with a central point source + fully resolved component, along with corresponding residuals (bottom panels).

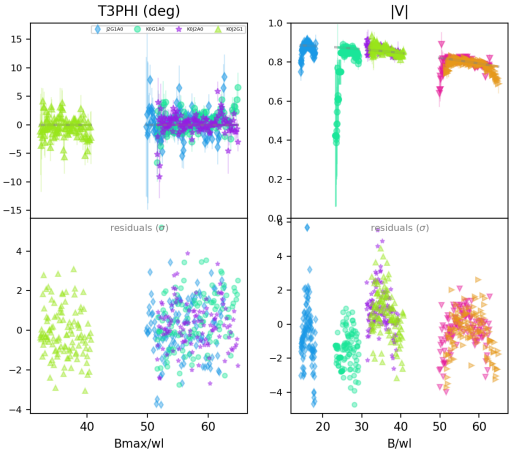

Fig. 16. |V|-T3PHI data (top panels) for WR 55 fit with a central point source + fully resolved component, along with corresponding residuals (bottom panels).

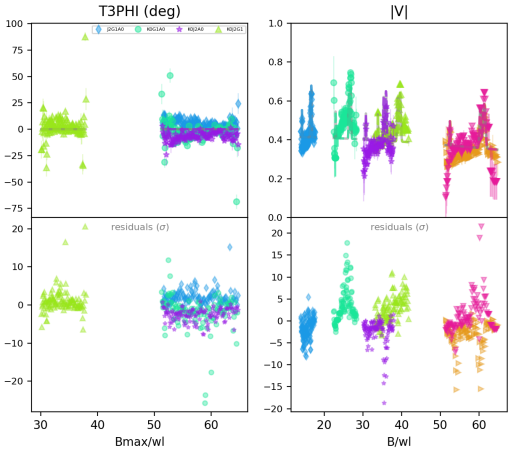

Fig. 17. |V|-T3PHI data (top panels) for WR 57 fit with a central point source + fully resolved component, along with corresponding residuals (bottom panels).

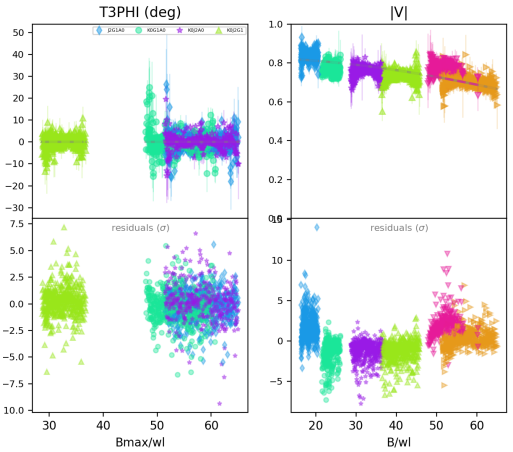

Fig. 18. |V|-T3PHI data (top panels) for WR 66 fit with a central point source + fully resolved component, along with corresponding residuals (bottom panels).

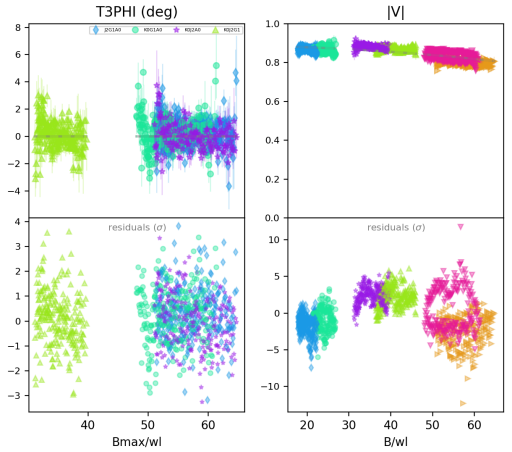

Fig. 19. |V|-T3PHI data (top panels) for WR 75 fit with a central point source + fully resolved component, along with corresponding residuals (bottom panels).

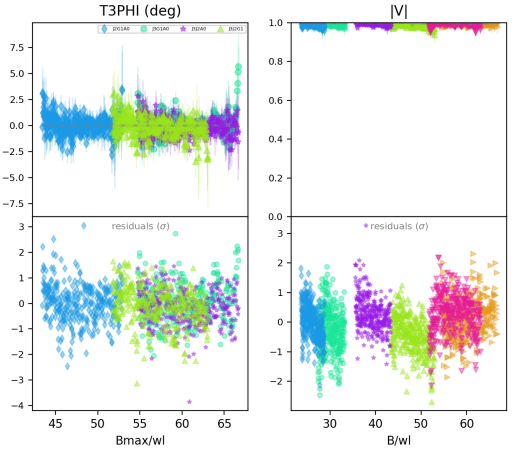

Fig. 20. |V|-T3PHI data (top panels) for WR 78 fit with only a point source, along with corresponding residuals (bottom panels).

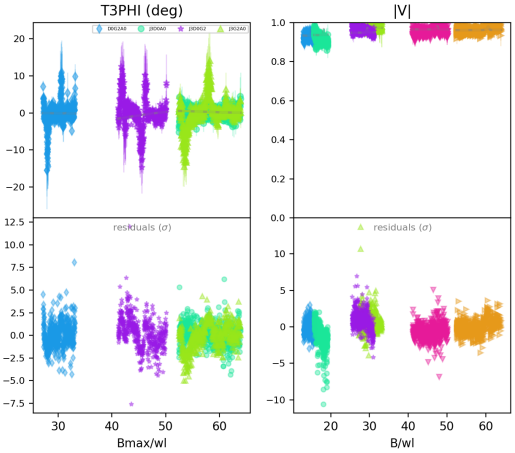

Fig. 21. |V|-T3PHI data (top panels) for WR 79 fit with a point source + fully resolved component, along with corresponding residuals (bottom panels).

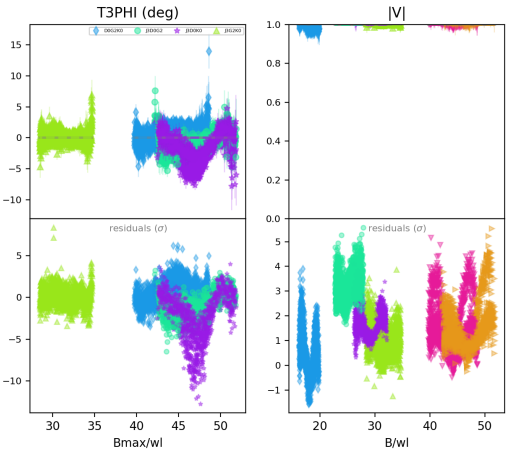

Fig. 22. |V|-T3PHI data (top panels) for WR 79a fit with an unresolved point source, along with corresponding residuals (bottom panels).

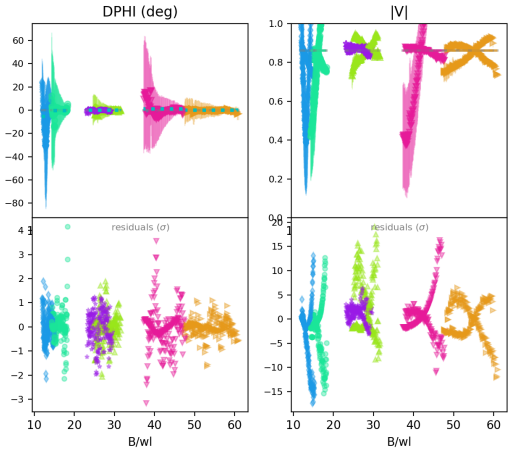

Fig. 23. |V|-T3PHI data (top panels) for WR 79b fit with an unresolved point source + fully resolved component, along with corresponding residuals (bottom panels).

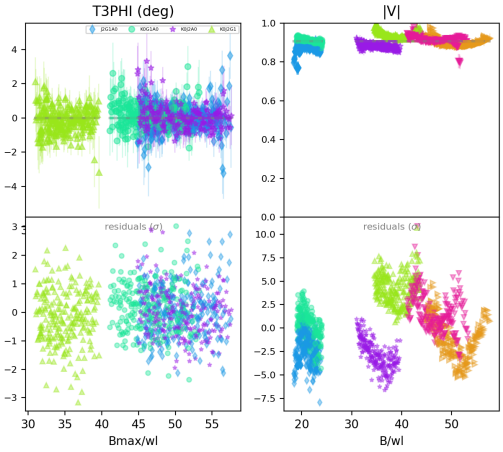

Fig. 26. |V|-T3PHI data (top panels) for WR 87 fit with a central point source + fully resolved component, along with corresponding residuals (bottom panels).

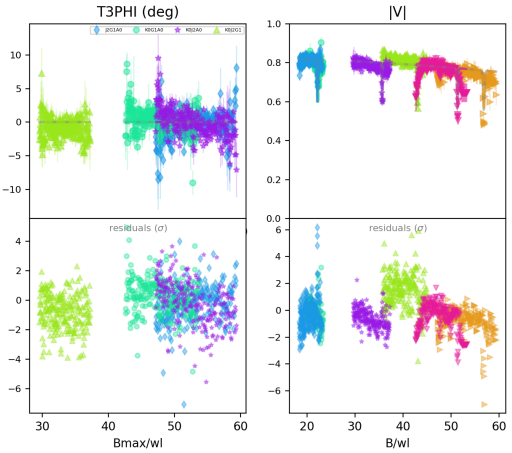

Fig. 24. |V|-T3PHI data (top panels) for WR 81 fit with a central point source + fully resolved component, along with corresponding residuals (bottom panels).

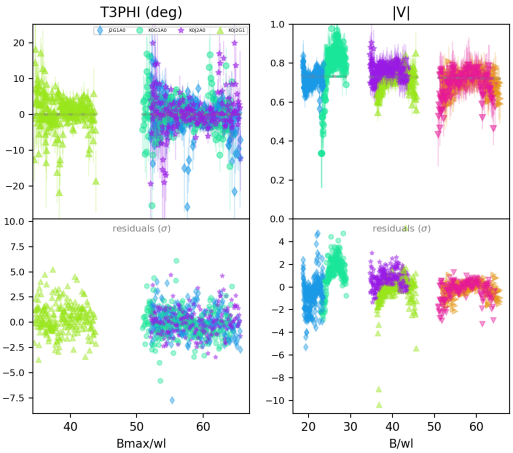

Fig. 27. |V|-T3PHI data (top panels) for WR 92 fit with a central point source + fully resolved component, along with corresponding residuals (bottom panels).

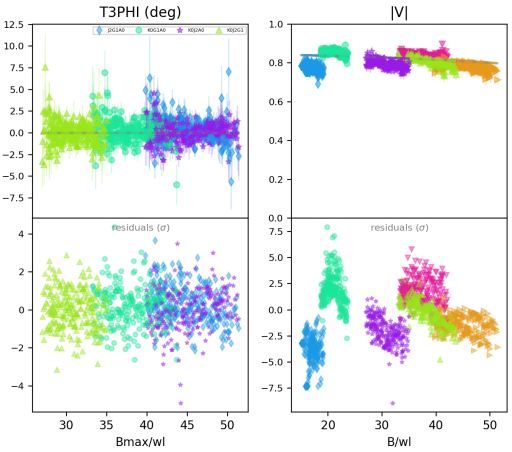

Fig. 25. |V|-T3PHI data (top panels) for WR 85 fit with a central point source + fully resolved component, along with corresponding residuals (bottom panels).

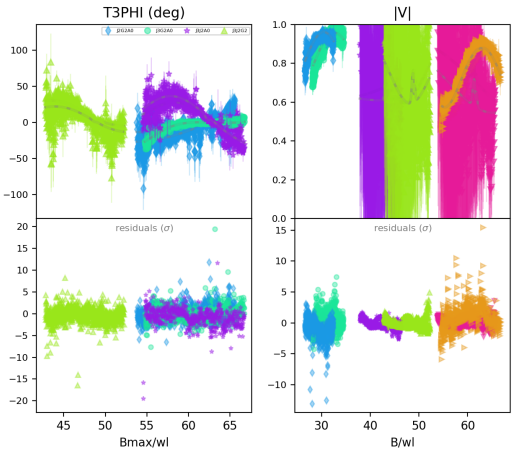

Fig. 28. |V|-T3PHI data (top panels) for WR 93 fit with two point sources to model the binary, along with a fully resolved component, and the corresponding residuals (bottom panels).

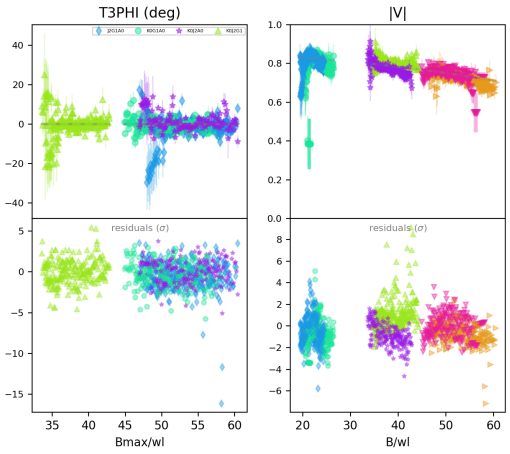

Fig. 29. |V|-T3PHI data (top panels) for WR 97 fit with a central point source + fully resolved component, along with corresponding residuals (bottom panels).

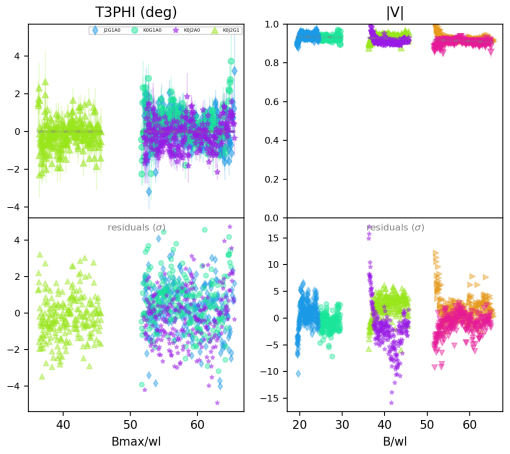

Fig. 30. |V|-T3PHI data (top panels) for WR 98 fit with a central point source + fully resolved component, along with corresponding residuals (bottom panels).

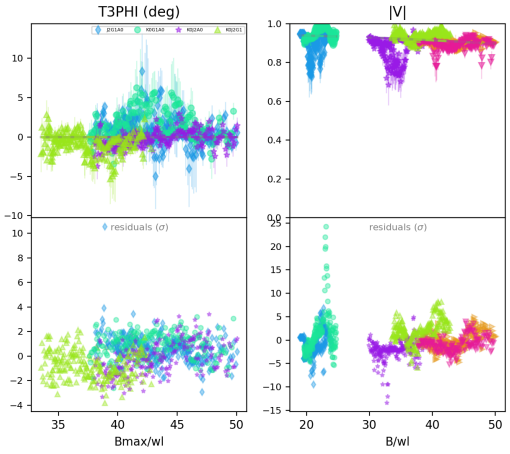

Fig. 31. |V|-T3PHI data (top panels) for WR 108 fit with a central point source + fully resolved component, along with corresponding residuals (bottom panels).

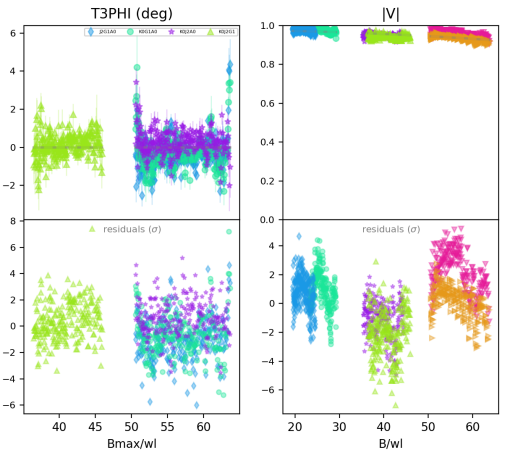

Fig. 32. |V|-T3PHI data (top panels) for WR 110 fit with a central point source + fully resolved component, along with corresponding residuals (bottom panels).

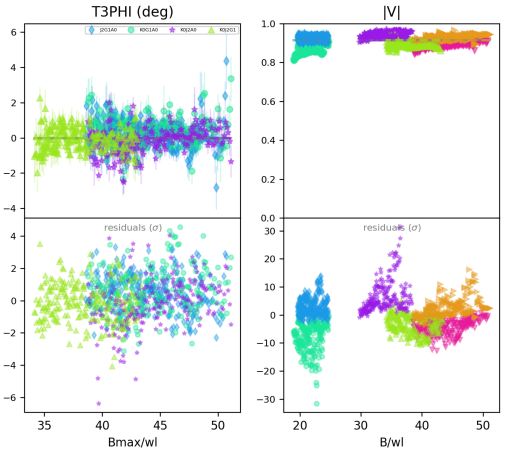

Fig. 33. |V|-T3PHI data (top panels) for WR 111 fit with a central point source + fully resolved component, along with corresponding residuals (bottom panels).

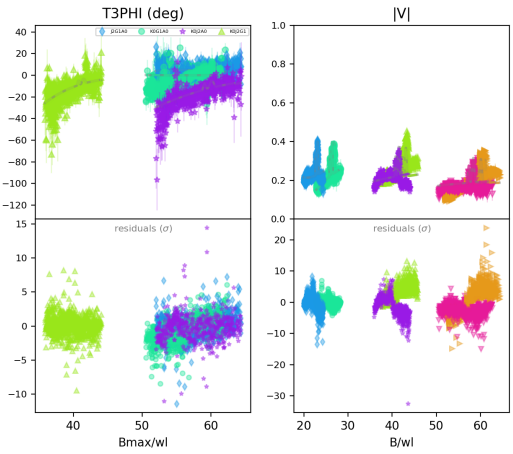

Fig. 34. |V|-T3PHI data (top panels) for WR 113 fit with a central point source + a very significant fully resolved component, along with corresponding residuals (bottom panels).

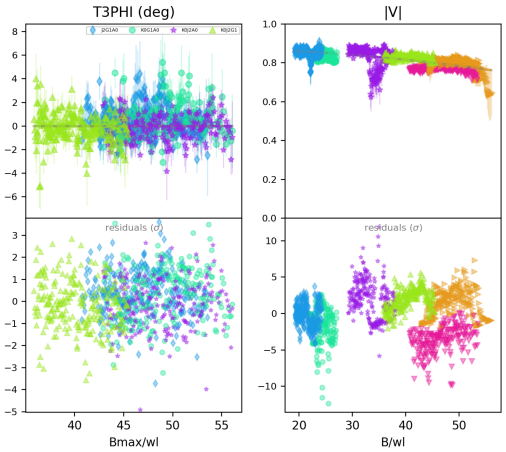

Fig. 35. |V|-T3PHI data (top panels) for WR 114 fit with a central point source + fully resolved component, along with corresponding residuals (bottom panels).

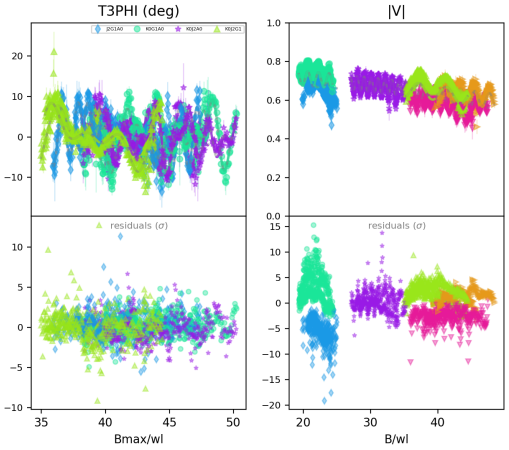

Fig. 36. |V|-T3PHI data (top panels) for WR 115 fit with two point sources to model the binary, along with a fully resolved component, and the corresponding residuals (bottom panels).

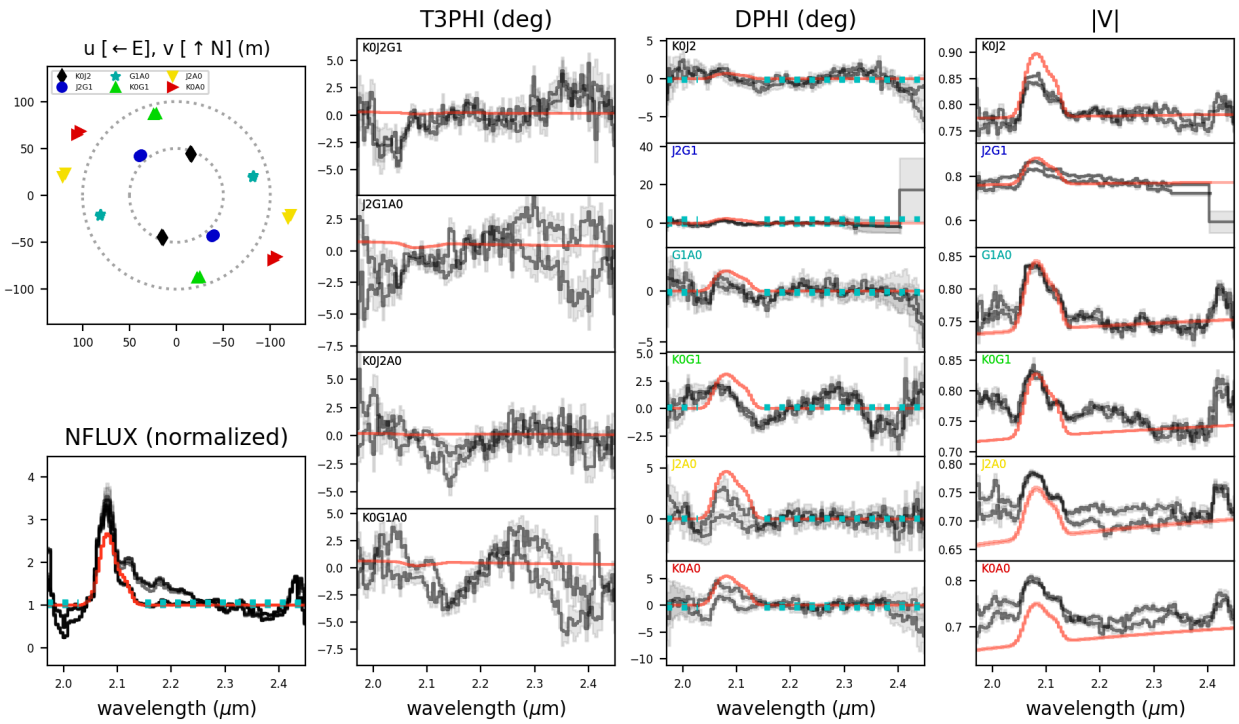

Fig. 37. Complete spectro-interferometric data for WR 9 with the best-fit model, similar to Figure 5 in the paper.

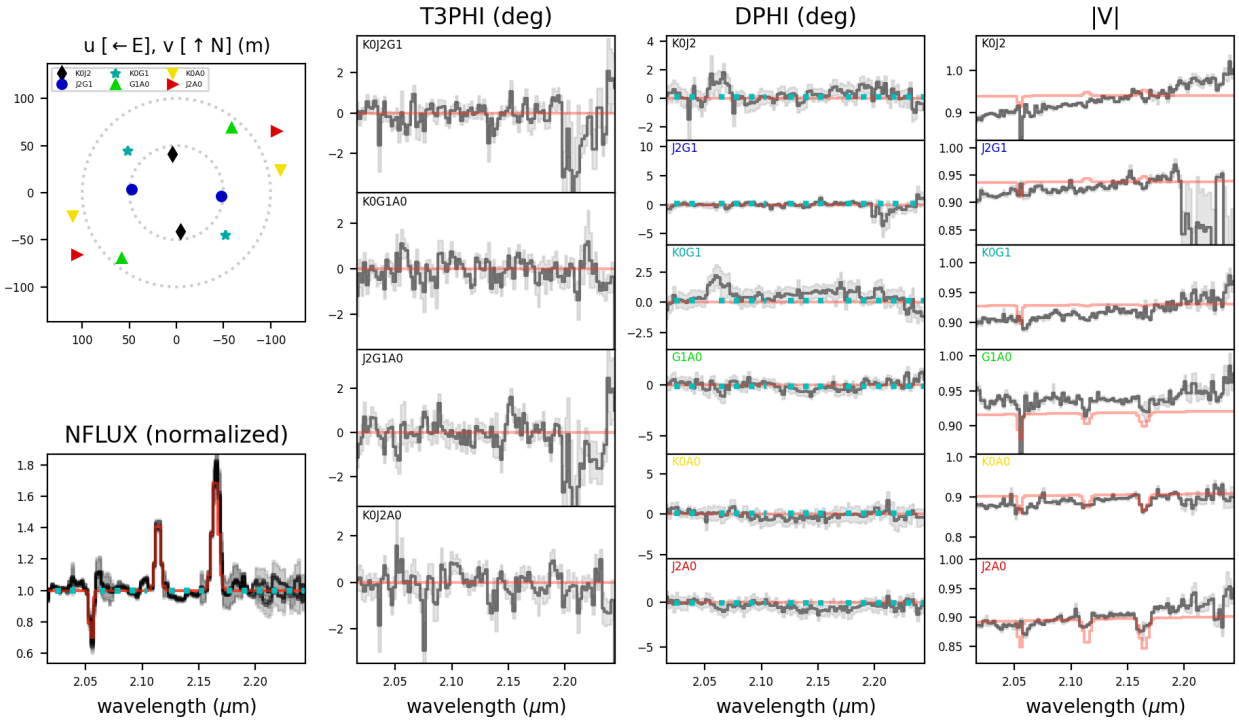

Fig. 38. A zoomed-in snippet of complete spectro-interferometric data for WR 16 with the best-fit model, similar to Figure 6 in the paper.

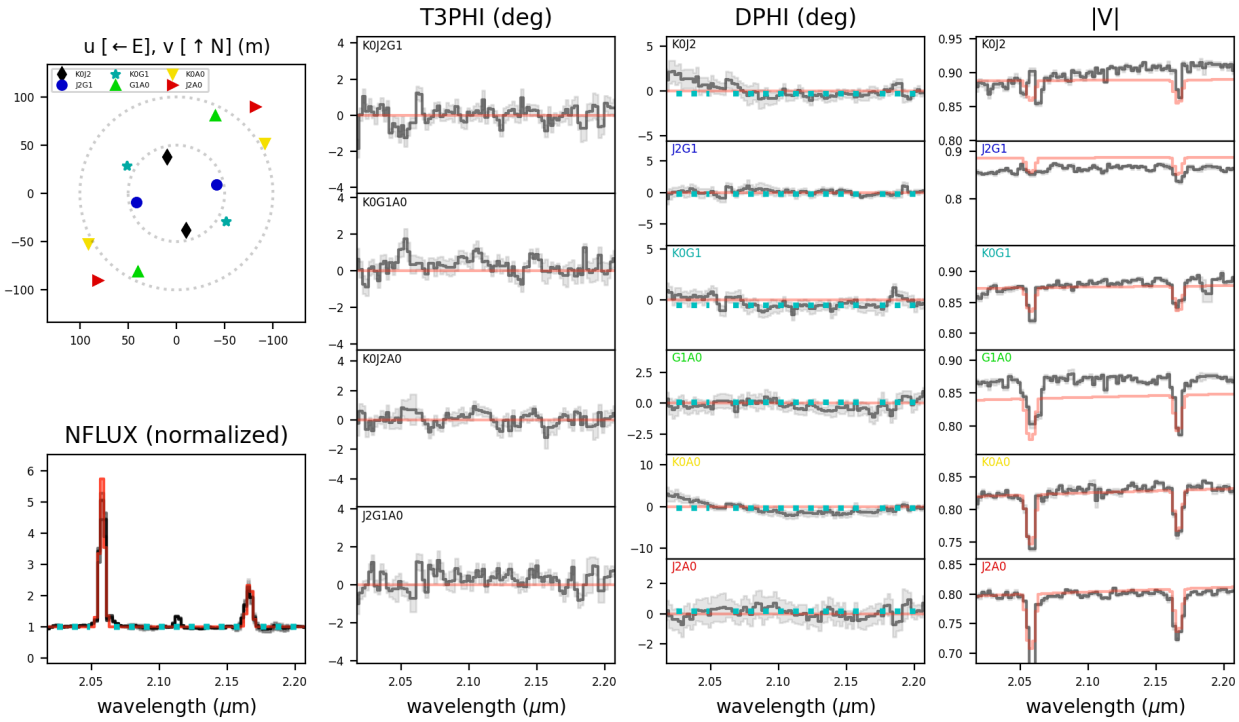

Fig. 39. A zoomed-in snippet of complete spectro-interferometric data for WR 31a with the best-fit model, similar to Figure 6 in the paper.

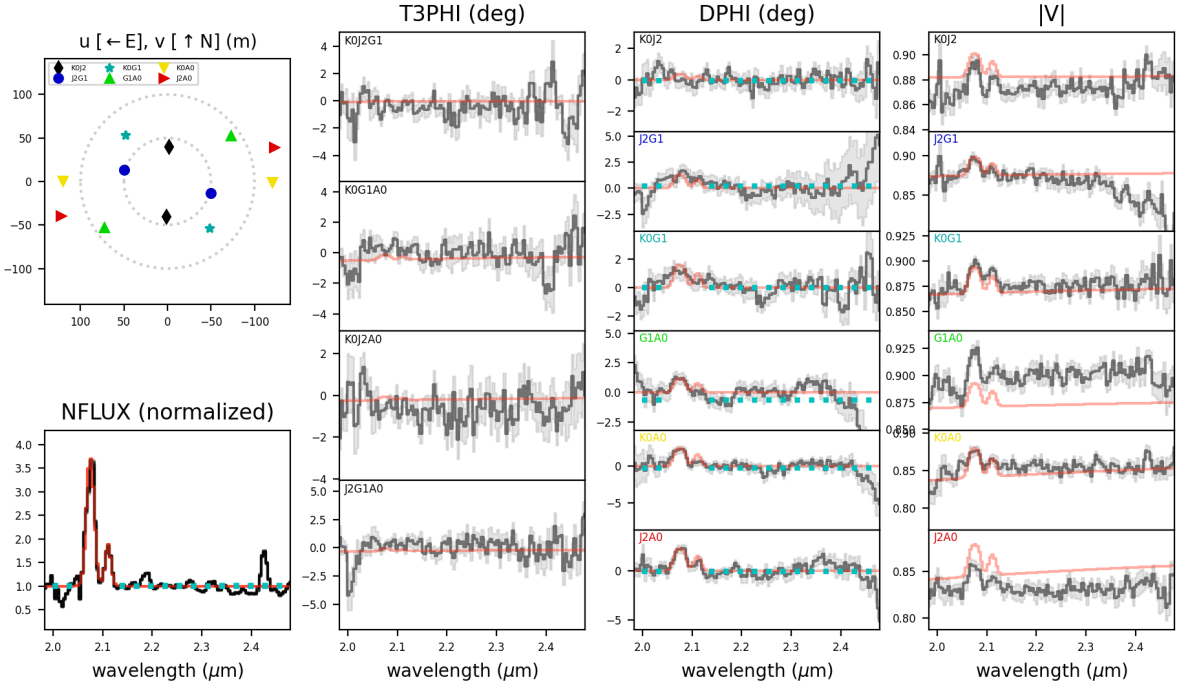

Fig. 40. Complete spectro-interferometric data for WR 42 with the best-fit model, similar to Figure 5 in the paper.

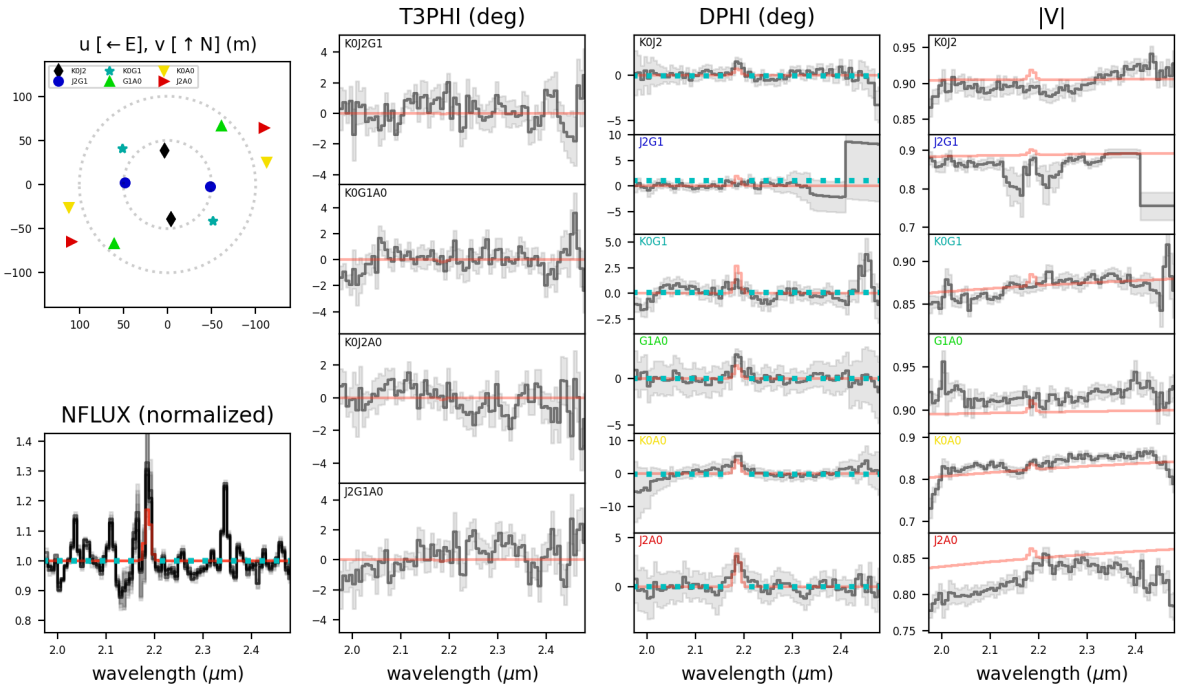

Fig. 41. Complete spectro-interferometric data for WR 47 with an approximate model (similar to Fig. 5 in the paper) over-plotted.

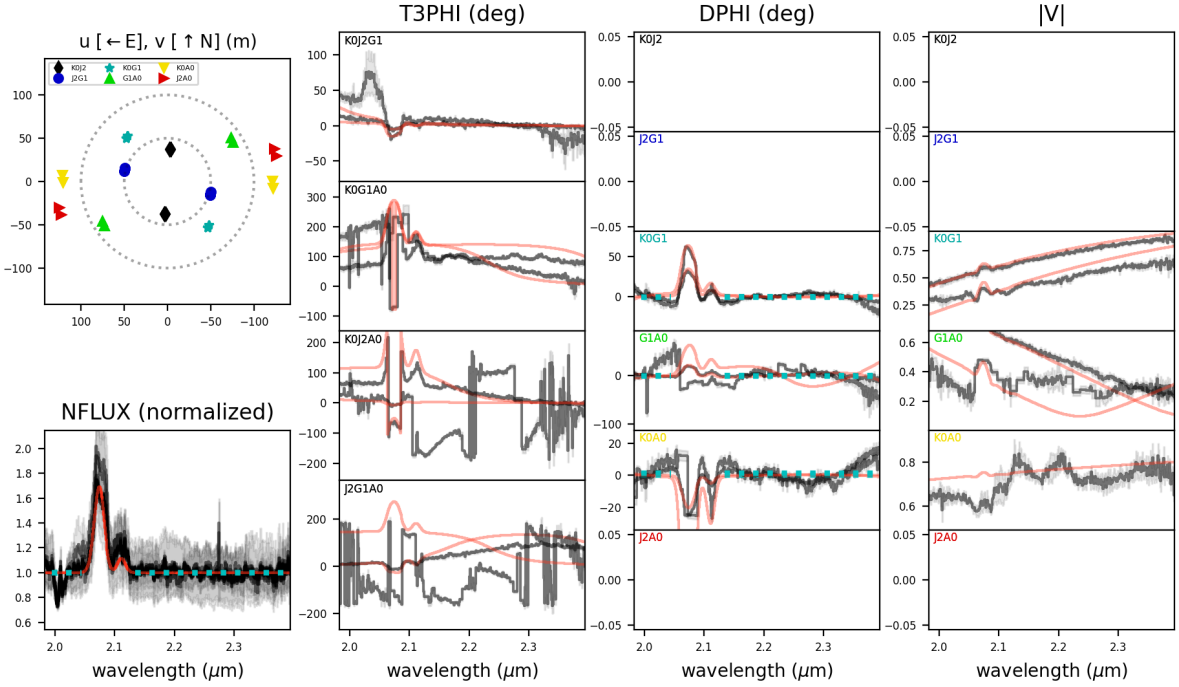

Fig. 42. Complete spectro-interferometric data for WR 48 with the best-fit binary model.

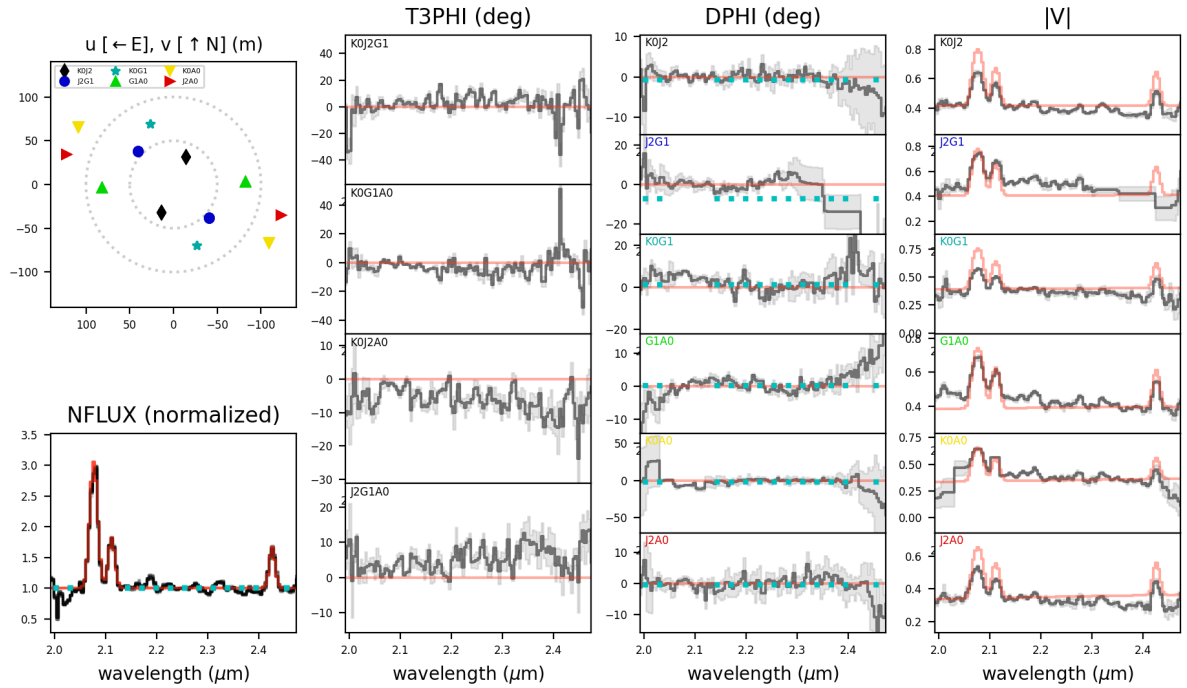

Fig. 43. Complete spectro-interferometric data for WR 57 with the best-fit model.

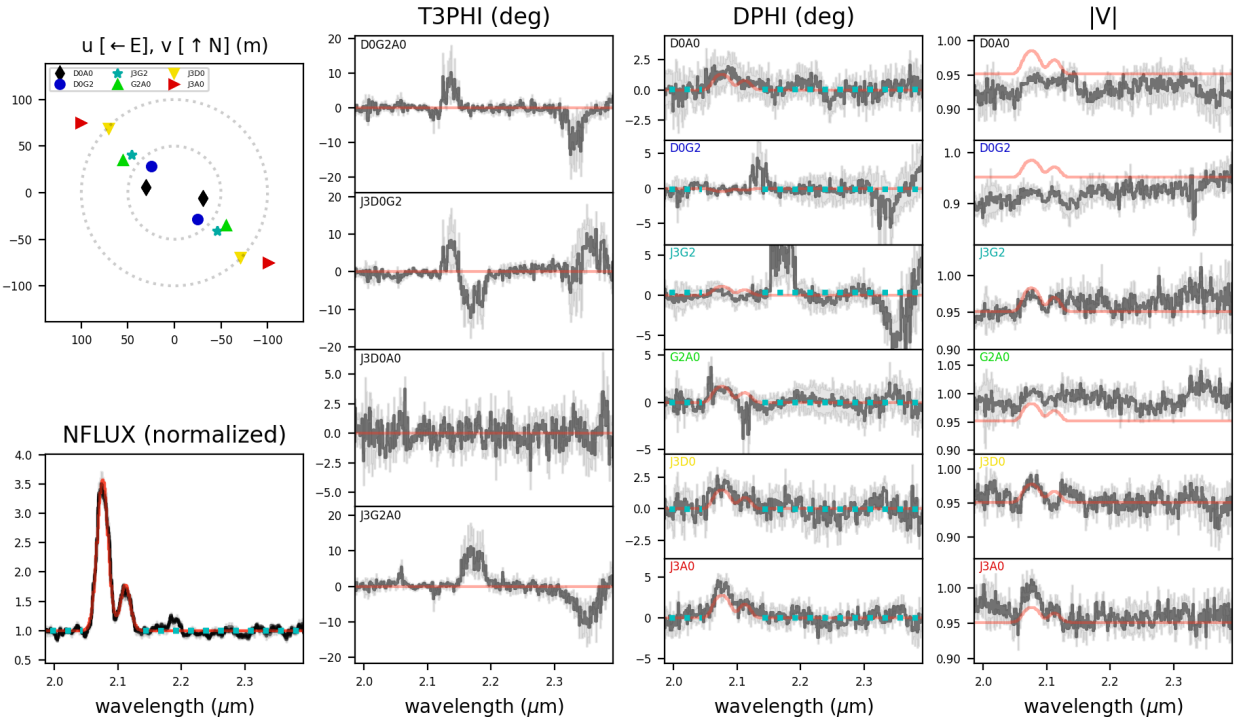

Fig. 44. Complete spectro-interferometric data for WR 79 with the best-fit model, similar to Figure 5 in the paper.

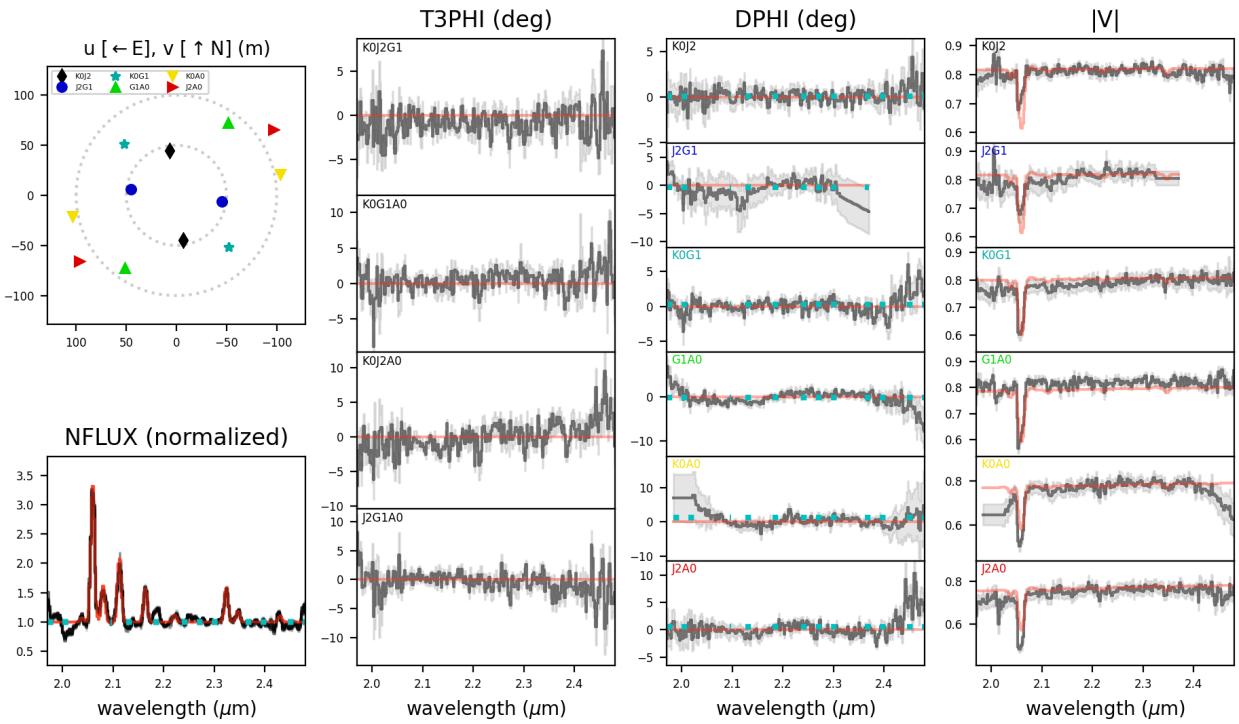

Fig. 45. Complete spectro-interferometric data for WR 81 with the best-fit model.

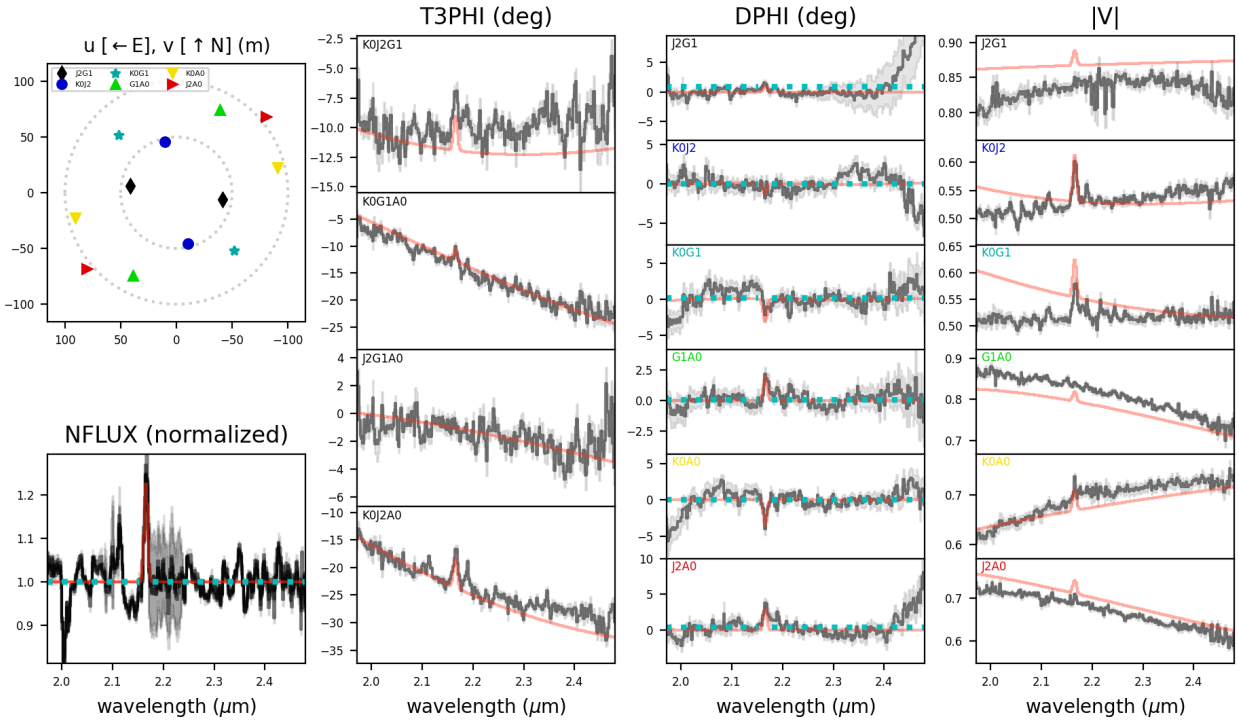

Fig. 46. Complete spectro-interferometric data for WR 89 with the best-fit binary model.

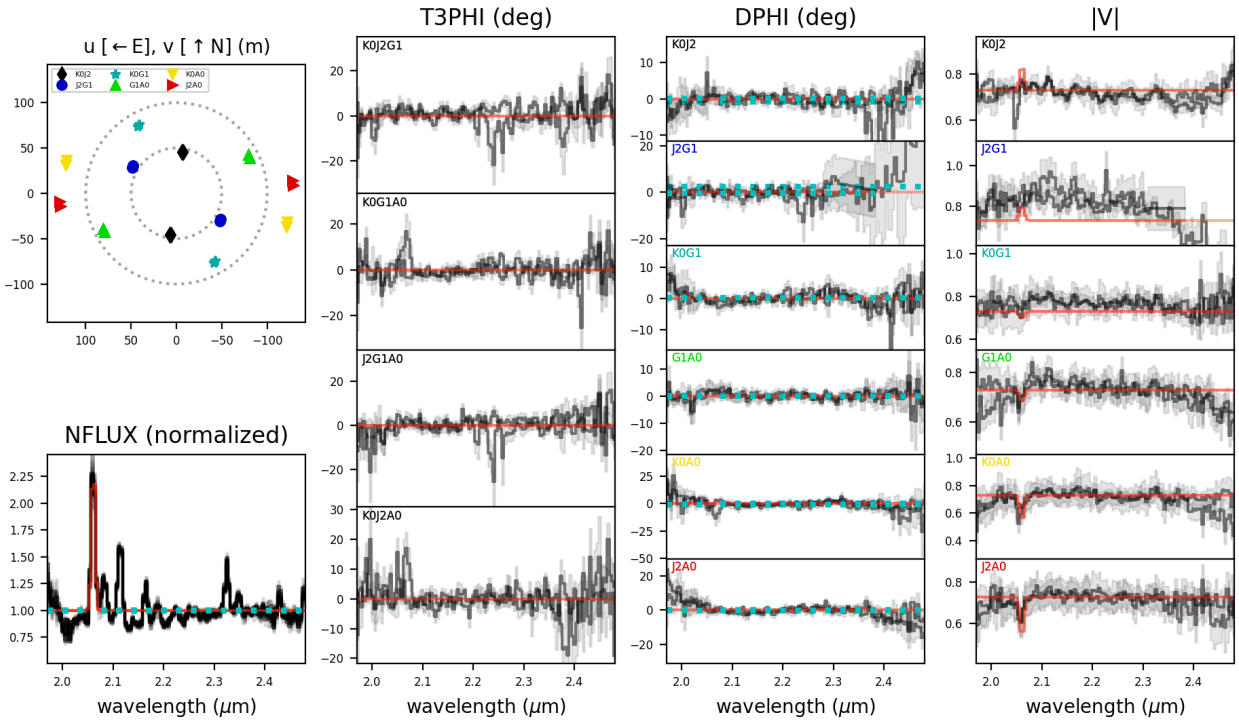

Fig. 47. Complete spectro-interferometric data for WR 92 with the best-fit model.

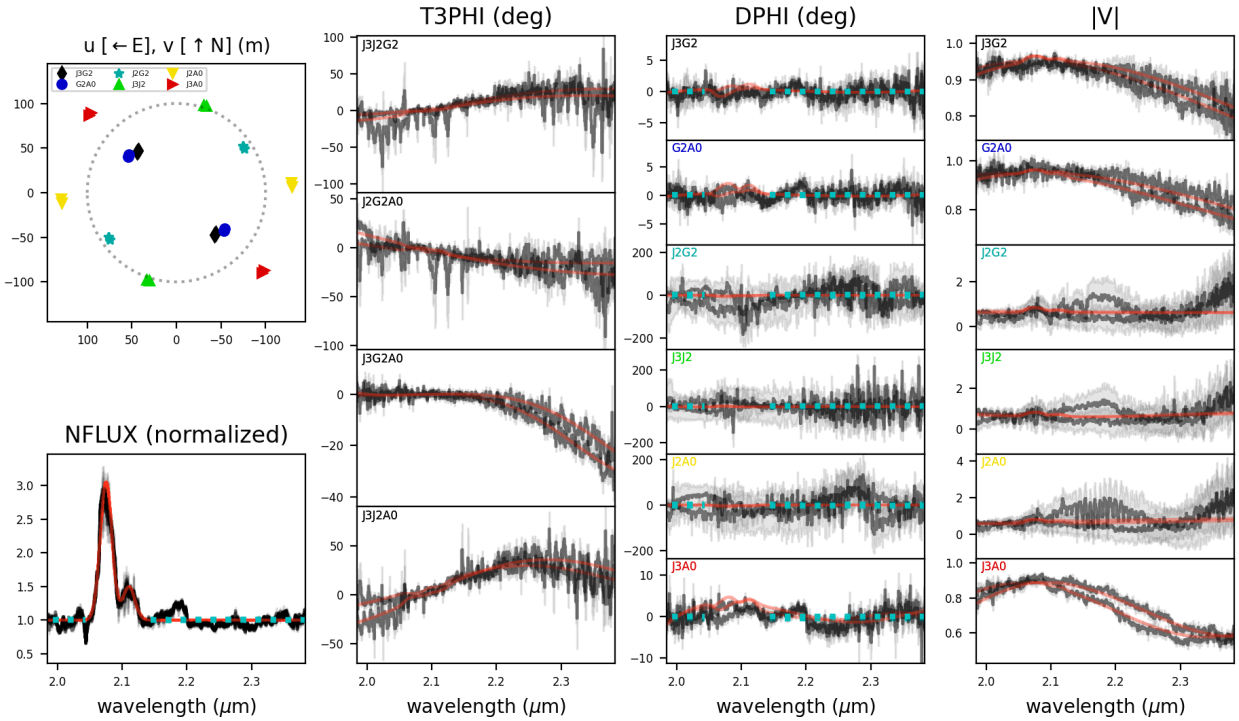

Fig. 48. Complete spectro-interferometric data for WR 93 with the best-fit binary model.

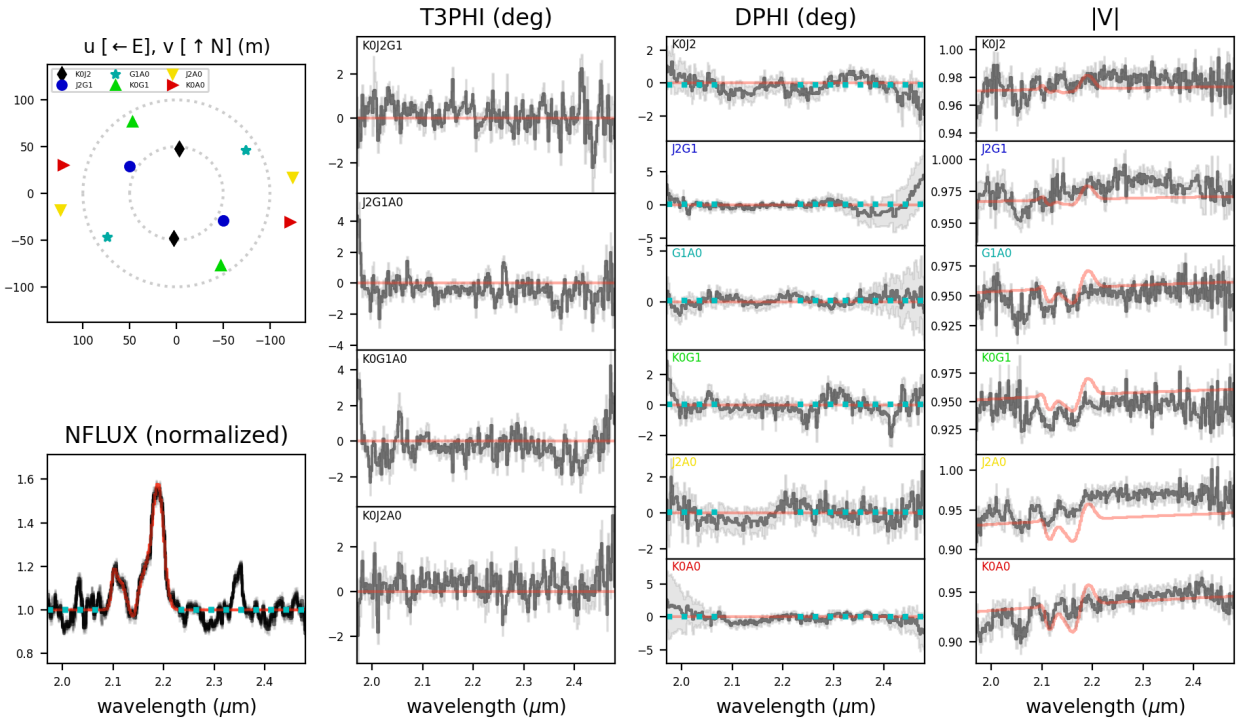

Fig. 49. Complete spectro-interferometric data for WR 110 with an approximate model (similar to WR 78) over-plotted.

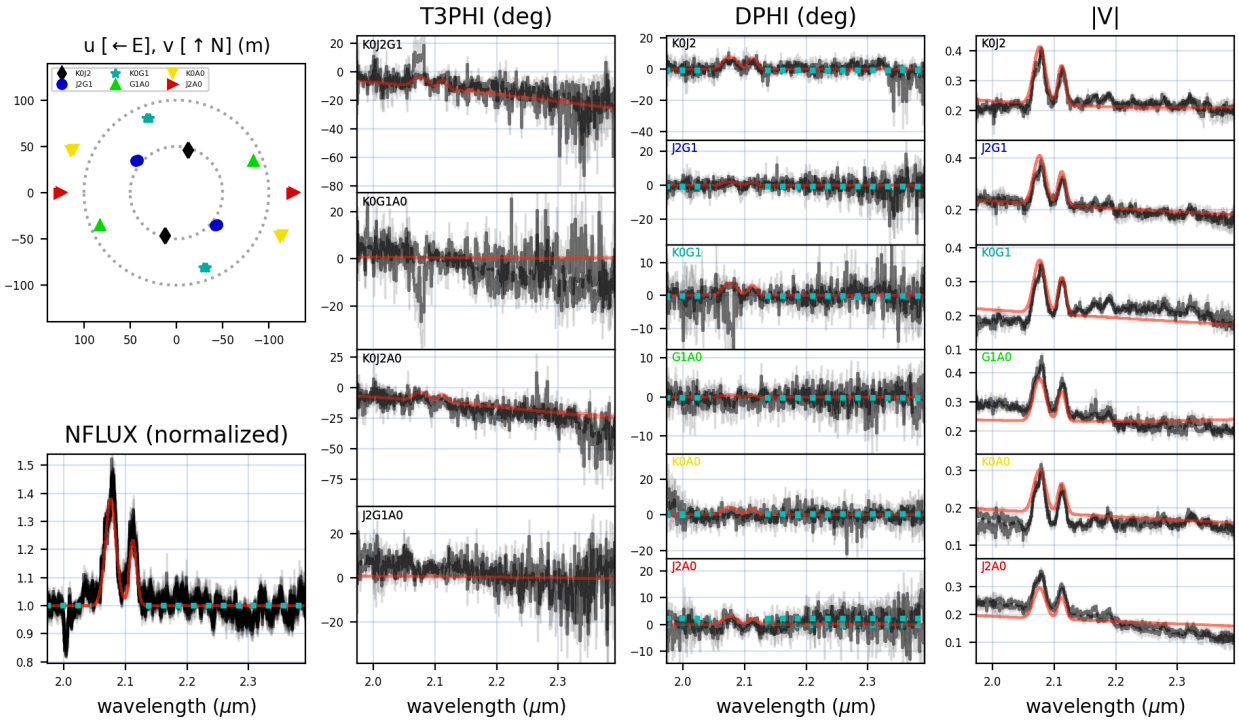

Fig. 50. Complete spectro-interferometric data for WR 113 with the best-fit model.

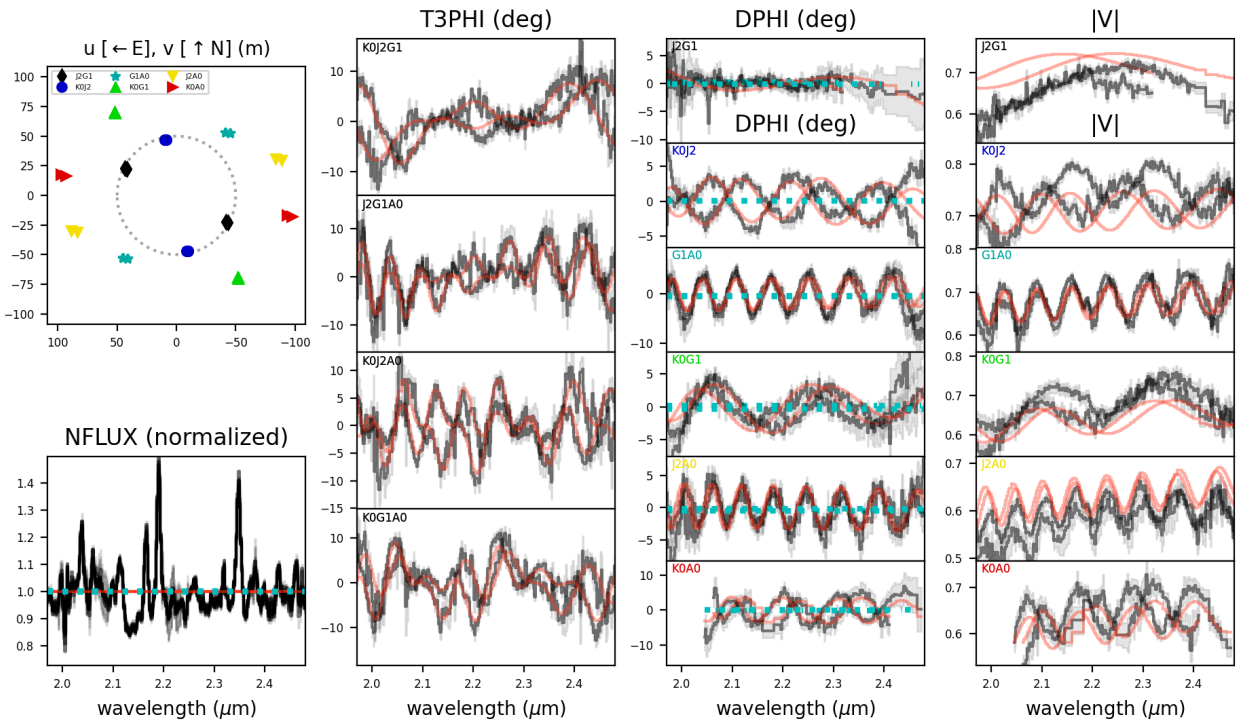

Fig. 51. Complete spectro-interferometric data for WR 115 with the best-fit binary model.